Langmuir

Article

pubs.acs.org/Langmuir

Surface Grafted Chitosan Gels. Part II. Gel Formation and Characterization

Chao Liu,[†] Esben Thormann,[‡] Per M. Claesson,[†,§] and Eric Tyrode[†,*]

[†]School of Chemical Science and Engineering, Department of Chemistry, Surface and Corrosion Science, KTH Royal Institute of Technology, Drottning Kristinas väg 51, SE-100 44 Stockholm, Sweden

[‡]Department of Chemistry, Technical University of Denmark, Kemitorvet 207, DK-2800 Kongens Lyngby, Denmark

[§]Chemistry Materials and Surfaces, SP Technical Research Institute of Sweden, P.O. Box 5607, SE-114 86 Stockholm Sweden

Supporting Information

ABSTRACT: Responsive biomaterial hydrogels attract significant attention due to their biocompatibility and degradability. In order to make chitosan based gels, we first graft one layer of chitosan to silica, and then build a chitosan/poly(acrylic acid) multilayer using the layer-by-layer approach. After cross-linking the chitosan present in the polyelectrolyte multilayer, poly(acrylic acid) is partly removed by exposing the multilayer structure to a concentrated carbonate buffer solution at a high pH, leaving a surface-grafted cross-linked gel. Chemical cross-linking enhances the gel stability against detachment and decomposition. The chemical reaction between gluteraldehyde, the cross-linking agent, and chitosan was followed in situ using total internal reflection Raman (TIRR) spectroscopy, which provided a molecular insight into the complex reaction mechanism, as well as the means to quantify the cross-linking density. The amount of poly(acrylic acid) trapped inside the surface grafted films was found to decrease with decreasing cross-linking density, as confirmed in situ using TIRR, and ex situ by Fourier transform infrared (FTIR) measurements on dried films. The responsiveness of the chitosan-based gels with respect to pH changes was probed by quartz crystal microbalance with dissipation (QCM-D) and TIRR. Highly cross-linked gels show a small and fully reversible behavior when the solution pH is switched between pH 2.7 and 5.7. In contrast, low cross-linked gels are more responsive to pH changes, but the response is fully reversible only after the first exposure to the acidic solution, once an internal restructuring of the gel has taken place. Two distinct pK_a's for both chitosan and poly(acrylic acid), were determined for the cross-linked structure using TIRR. They are associated with populations of chargeable groups displaying either a bulk like dissociation behavior or forming ionic complexes inside the hydrogel film.

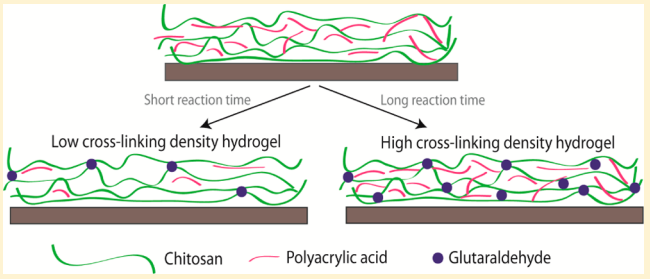

1. INTRODUCTION

Polymer hydrogels have attracted attention for the past several decades due to their stimuli responsive properties that can lead to large volumetric changes. This can, for instance, be utilized for loading and releasing active molecules in drug delivery applications, and for modification of surface properties such as adhesion and friction.[1,2] The volumetric change of a hydrogel can be induced by a range of stimuli, such as pH, salt concentration, or temperature. Unlike a hydrogel particle that is able to swell in three dimensions, a hydrogel film can only swell in one dimension. This swelling dimensionality is the same as that for grafted polymer and polyelectrolyte brushes; however, the hydrogel thin films are distinguished by the presence of covalent cross-links. Hydrogel thin films have shown great potential in the fabrication of miniaturized devices with fast response times and storage function.[1]

Hydrogel films are common in nature. For instance, mucous hydrogels cover almost all internal surfaces in the body and function as protective barriers against, e.g., viruses, bacteria and/or dehydration, but can also act as lubricating layers.[3] The sophisticated nanostructured and porous cartilage that covers the bone ends in articulated joints can be regarded as a relatively stiff hydrogel, and its mechanical responses to pressure changes are important for joint lubrication.[4] In both these examples, large glycoproteins that contain heavily glycosylated regions fulfill important roles related to their strong interaction with water.[5] For this reason hydrogels containing polysaccharides have attracted attention, and they are, for instance, used in the regeneration of plant and human tissues.[6] Chitin is one of the most abundant polysaccharides in nature, and chitosan (CHI) is produced by alkaline deacetylation of chitin, and it has been reported to be nontoxic, antigenic, biocompatible, and degradable.[7−10] The hydroxyl and amine groups of chitosan are important for the interactions with water. Due to the high content of primary amines, chitosan is a cationic polyelectrolyte in neutral and acidic solutions, making chitosan microcapsules responsive to external stimuli such as pH and ionic strength changes. Such

Received: April 9, 2014
Revised: July 6, 2014
Published: July 9, 2014

microcapsules have been suggested as being promising in controlled release applications.[11,12]

In our previous work we analyzed the formation of surface grafted chitosan/PAA multilayers using layer-by-layer assembly.[13] We find, as expected, that electrostatic interactions are key to fabrication of such multilayers. However, the formation process is quite complex including diffusion of components within the multilayer and formation of islands that lead to nonlinear growth. In this work we use glutaraldehyde, which has been reported to cross-link chitosan films effectively,[14] to induce cross-links between the chitosan molecules in the multilayer. The approach consisting in cross-linking polyelectrolyte multilayers containing chitosan to create films with varying mechanical and stimuli responsive properties has been extensively reported in the literature.[15−18] Here we are specifically concerned in creating a surface grafted chitosan hydrogel, for which the low molecular weight PAA present in the multilayer has to diffuse out of the film. The extent of PAA leaving the film depends on the cross-linking density, and if the cross-linking density is sufficiently low, a surface grafted cross-linked chitosan gel is achieved. To follow the cross-linking reaction in situ and determine the composition of the resulting chitosan-dominated hydrogel, we use total internal reflection Raman (TIRR). Moreover, Fourier transform infrared spectroscopy (FTIR) is also utilized to obtain ex situ complementary information. Finally, TIRR combined with quartz crystal microbalance with dissipation (QCM-D) is used to investigate the stability and responsiveness of the gels with respect to pH and ionic strength changes, and provide molecular insight into the degree of dissociation of the chargeable groups inside the hydrogel.

2. MATERIALS AND METHODS

2.1. Materials. The chitosan (CHI) employed in this study has a degree of deacetylation of 75-85% and a molecular weight in the range 50 000−190 000 g/mol, based on viscosity measurements. Both chitosan and poly(acrylic acid) (PAA) with molecular weight 1800 g/mol were purchased from Sigma-Aldrich. Fifty weight percent glutaraldehyde aqueous solution (GA), glacial acetic acid (HAc), sodium hydroxide (NaOH) pellets (99.99% purity), hydrochloric acid (HCl, ACS reagent grade), sodium chloride (99.5% purity), sodium carbonate (99.5% purity), and sodium bicarbonate (99.5% purity) were used as received from Sigma-Aldrich. The water used was purified by a Milli-Q Plus system (resistivity of 18.2 MΩ cm, and the total organic carbon content lower than 3 ppb).

2.2. Preparation of Surface-Grafted Chitosan Gels. The preparation of the surface grafted CHI/PAA polyelectrolyte multilayer has been described in detail in part I of this series of papers.[13] The chitosan molecules in multilayers formed by 11 chitosan and 10 PAA deposition steps, referred to as 11/10 chitosan/PAA, was selectively cross-linked in a 2.5 wt % glutaraldehyde solution by a Schiff's base reaction carried out at 21 °C. The cross-linked films exhibit a characteristic brown color when visually inspected.[19,20] The cross-linking density was changed by varying the reaction time between 5 min and 24 h. A large fraction of the PAA was removed from the cross-linked film by overnight treatment with 0.2 M carbonate buffer at pH 9, and this process was repeated twice using fresh carbonate buffer solutions.

2.3. Characterization Methods. Silica-coated quartz crystals for QCM-D experiments and thermally oxidized silicon wafers for the FTIR and atomic force microscpy (AFM) measurements were treated with 2% Hellmanex (Hellma GmbH) for 30 min and then rinsed with copious amount of Milli-Q water. The custom-made fused silica hemispheres (CVI-Melles Griot) employed in the TIRR measurements were soaked in bichromatic sulfuric acid for 30 min prior to being flushed with water.

2.3.1. Total Internal Reflection Raman (TIRR) Spectroscopy. Our home-built TIRR instrument has been described in detail elsewhere.[21] The plane side of the hemisphere was sealed with a Viton O-ring on the top of a custom-made glass cell. Inside the cell under the center of the hemisphere, a glass capillary served as the inlet for solution injection. During the data acquisition, the solution in the cell was stagnant by closing the inlet and outlet valves. The nominal power at the laser head was in most of the experiment kept constant at 200 mW, which, when considering the beam size at the sample surface, was equivalent to ∼200 W/mm^2. However, for tracking the cross-linking reaction of the multilayer with glutaraldehyde, the power densities were dropped to ∼15 W/mm^2, as laser powers higher than ∼50 W/mm^2 appeared to have an effect on the reaction kinetics. The angle of incidence at the silica−water interface, θ, was set to 72.0°, which is larger than the critical angle of 65.6°. This results in a penetration depth (d) of the squared evanescent field of about 105 nm. The incident laser was S polarized (perpendicular to the plane of incidence) in all experiments, since this polarization gave the highest signal levels. We also selected a single polarization of the scattered radiation, Sy, due to the stronger Raman tensor elements probed under this polarization.[22,23] The acquisition time for each Raman spectrum varied between 30 s and 8 min depending on the experiment.

2.3.2. Transmission Fourier Transform Infrared Spectroscopy. The FTIR spectra were recorded in a transmission configuration with 4 cm^{-1} resolution in a Spectrum One, PerkinElmer FTIR spectrometer. The temperature was kept constant at 25.0 °C, and to improve the signal-to-noise ratio, a minimum of 25 scans were averaged. The samples consisted of polyelectrolyte multilayers and/or cross-linked chitosan gels deposited on IR-transparent silicon wafers. During the measurements the samples were placed in a dry air-purged compartment inside the spectrometer. Note that, in contrast to TIRR, transmission IR measurements were collected ex situ and under dry conditions.

2.3.3. Atomic Force Microscopy. Topographical images of surface grafted CHI gels were obtained by using a Multimode Nanoscope V atomic force microscope (Bruker, USA) operated in PeakForce tapping mode in air at 25 °C. A triangular silicon nitride cantilever (ScanAsyst Air, Bruker), with a nominal spring constant of 0.4 N/m, a resonance frequency of 70 kHz and a tip radius of 2 nm was used. The NanoScope Analysis version 1.20 (Bruker) software was employed to analyze the images, and all the topography images were flattened to remove tilt.

2.3.4. Quartz Crystal Microbalance with Dissipation. A QCM-D E4 device, from Q-sense AB (Gothenburg, Sweden) was used to simultaneously measure the resonant frequency shift, Δf, and the change in energy dissipation, ΔD, at several overtones. The AT-cut crystals coated with a 50 nm silica layer had a fundamental shear frequency of 5 MHz. The data were analyzed using three different models, briefly described below, to evaluate the mass attached to the sensor's surface. This mass is referred to as the sensed mass, m_s, when the measurement is conducted in aqueous environment since both the adsorbed species and hydrodynamically coupled water contributes to the measured mass. The water content of the layer was calculated from the sensed mass and the mass of the layer determined in air.

The Sauerbrey model is appropriate when the film is thin, rigid, and evenly distributed over the sensor surface. In this case, the frequency change is proportional to the sensed mass as[24]

$$m_s = -\frac{C \cdot \Delta f}{n} \quad (1)$$

where C is the mass sensitivity factor which equals 17.7 ng Hz^{-1} cm^{-2} for our sensors and n is the overtone number (1, 3, 5, 7...). The acoustic shear waves associated with the different overtones penetrate the solution outside the sensor to different depths, with a decay length ranging from 140 nm (n = 3) to 65 nm (n = 13) in water at 25 °C.[25]

The Sauerbrey model is not appropriate for viscoelastic layers, therefore other models have to be used. In this work we employed the Johannsmann model,[26] which uses data from several overtones to create a regression line from which the sensed mass is derived as

dx.doi.org/10.1021/la501319r | Langmuir 2014, 30, 8878−8888

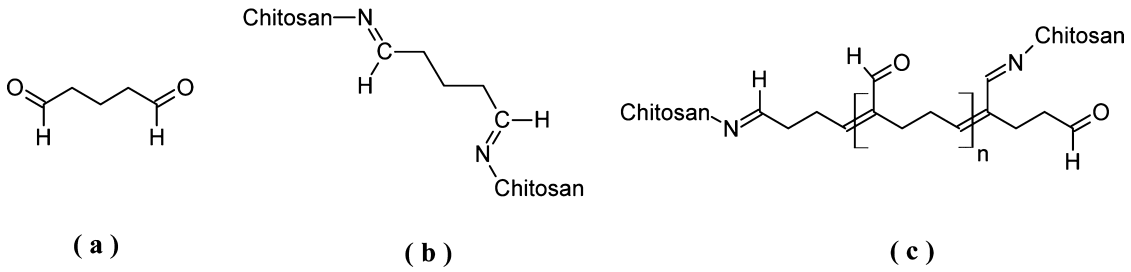

Figure 1. Molecular structure of (a) glutaraldehyde in its monomeric form, (b) amine groups of chitosan cross-linked by a simple Schiff base on both ends of the monomeric glutaraldehyde (unstable under acidic conditions), and (c) one of the likely cross-linking reaction products between a polymeric form of glutaraldehyde and chitosan, which allow for multiple connections with chitosan moieties (note the conjugate system consisting of a Schiff base and an adjacent ethylenic double bond).

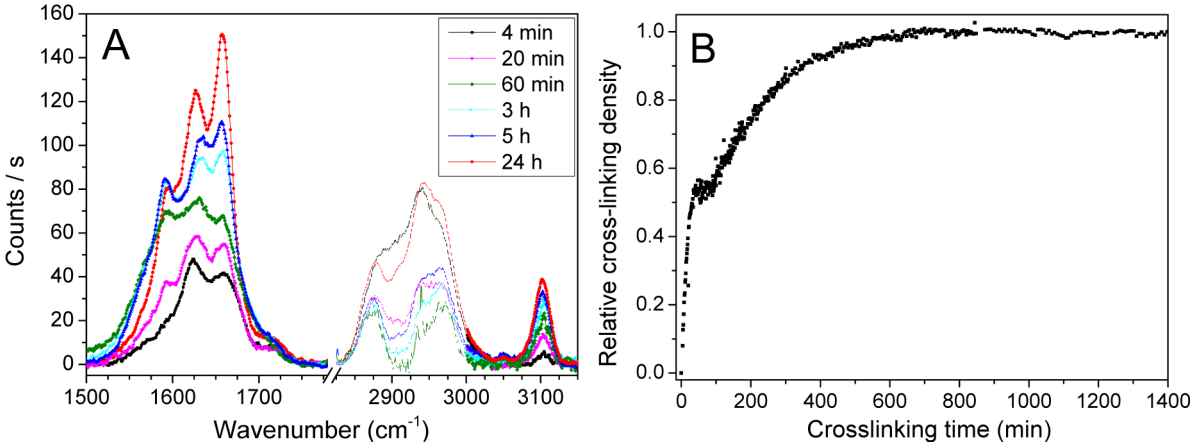

Figure 2. (a) Selected TIRR spectra during the cross-linking reaction of chitosan with glutaraldehyde. Contributions from the chitosan/PAA multilayer have been removed by subtracting the spectrum of the multilayer prior to the addition of glutaraldehyde. Fluorescence, which gave rise to sloping backgrounds in the early stages of the reaction, was also manually subtracted. Note the break in the spectrum between 1775 cm^{-1} and 2825 cm^{-1}. (b) Relative cross-linking density (fraction of imine groups in the grafted gel) as a function of time estimated from the C−H stretching mode of the hydrogen attached to the unsaturated carbon forming the Schiff base (see text for details). Data originates from analysis of 440 spectra collected in a 24 h period.

$$m_s = m_j\left[1 + J(f)\frac{\rho d^2\omega^2}{3}\right] \quad (2)$$

where ρ is the film density, d is the thickness, ω is the angular frequency, and J is the viscoelastic compliance. This model is appropriate when the viscoelastic compliance is frequency independent, and in such a case the sensed mass, m_j, is obtained from the intercept of the m_s versus ω^2 plot at zero frequency.

The QCM-D data were also analyzed using the Voigt viscoelastic model,[25] where the viscoelastic response of the film is represented by an elastic component in parallel with a viscous component. In this case, the software Q-tools provided by Q-sense was utilized, and the sensed mass is referred to as m_v.

From the QCM-D data we calculate the dry mass and sensed mass (wet mass) of the gel films. This is done by first determining the frequency and dissipation values of the uncoated crystal in air and in water. Next, the film is formed on the sensor surface and the dry and sensed mass is determined from the frequency and dissipation shifts relative to the uncoated crystal in the two environments. This procedure requires mounting, dismounting, and remounting of the sensor surface in the QCM-D device, which constitutes a source of error. The magnitude of this error was determined by mounting and dismounting the bare crystals four times and comparing the frequency values, which resulted in a standard deviation in frequency of 25 Hz that corresponds to 4.4 mg/m^2 in the Sauerbrey model. The standard deviation for the dissipation is below 0.2×10^{-6}. The weight fraction of water, X_w, in the film was then calculated from dry (m_{dry}) and wet (m_{wet}) sensed masses:

$$X_w = \frac{m_{wet} - m_{dry}}{m_{wet}} \quad (4)$$

3. RESULTS AND DISCUSSION

3.1. Stability of the Multilayer Film Prior to Cross-Linking. QCM-D was used to evaluate the stability of the multilayer film upon changes in solution conditions prior to addition of the cross-linking agent. As clearly shown in the Supporting Information (Figure S1), the multilayer tends to dissolve in low pH and high ionic strength salt solutions, specifically when cycling the pH between 5.7 at 2.7 in a 100 mM NaCl solution. The disintegration of the multilayer is a consequence of reduced electrostatic interaction between chitosan and PAA,[27,28] since at pH 2.7 the chitosan segments (bulk $pK_a \approx 6.0-6.5$) are positively charged, whereas the PAA segments (bulk $pK_a \sim 4.8$) are largely neutralized. Thus, under acidic conditions the multilayer becomes unstable due to internal charge imbalance, resulting in film decomposition. We note that the first chitosan layer, which was grafted to the surface, remains intact.

3.2. Cross-Linking of the Chitosan/Poly(acrylic acid) Multilayer. The stability of the film can be dramatically improved by cross-linking specific segments in the multilayer. Here we make use of glutaraldehyde as cross-linking agent. This linear dialdehyde molecule (Figure 1a) is frequently used in a

dx.doi.org/10.1021/la501319r | Langmuir 2014, 30, 8878−8888

number of different applications due to its versatility, low cost, and high reactivity.[29] Glutaraldehyde is expected to react with the amine groups of chitosan, forming a stable C═N imine group (Schiff base). The reaction mechanism is, however, complex and not well understood, starting with the fact that in aqueous solutions, glutaraldehyde is not only found as a monomeric aldehyde (see Figure 1a), but it is also in equilibrium with different hydrated and cyclic isomeric forms.[24,30,31] Moreover, it can also easily polymerize in alkaline conditions through aldol reactions and condensations forming products with molecular masses of up 20 000 Da.[32] In our starting reaction solution (pH ∼ 4), such polymeric compounds with ethylenic double bonds were absent, as confirmed by the Raman spectrum of the bulk solution (see Figure S2 in the Supporting Information).

Nevertheless, when in contact with chitosan, and in parallel with the cross-linking reaction that forms the Schiff base, amino groups from chitosan are presumed to catalyze the aldol condensation/polymerization reaction forming irregular oligomeric products with aldehydes groups that can further react with other amino groups in neighboring chitosan segments.[29,31] The final cross-linking structure would then consist of aldol-condensed oligomers of glutaraldehyde with several imine linkages branching off and constituting conjugate systems with adjacent ethylenic (C═C) double bonds (see, for example, Figure 1c).[29−31] Here we make use of TIRR to provide a molecular insight into the reaction mechanism.

3.2.1. Cross-Linking Reaction Kinetics Obtained from TIRR. The cross-linking reaction after addition of glutaraldehyde to a multilayer film consisting of 11 layers of chitosan and 10 layers of PAA, was tracked in situ by TIRR. Selected spectra recorded as the reaction proceeds are presented in Figure 2a. Note that the bands shown originate exclusively from the cross-linking action of glutaraldehyde, as spectral contributions from the chitosan/PAA multilayer were removed by subtraction. Large changes are observed from the first recorded spectrum, 4 min after addition of the glutaraldehyde solution.

In the double bond stretching region, four bands can be clearly resolved. The first, centered at ∼1595 cm^{-1}, is assigned to a C═C stretch and confirms that aldol-condensed oligomers are formed (see Figure 1c). The relatively low peak position is explained by the effect of conjugation with the adjacent imine/carbonyl group, which weakens the double-bond force constant. The second band centered at ∼1630 cm^{-1} is associated with the Schiff base (C═N stretch) forming the conjugate system with the ethylenic bond mentioned above (see, for example, the Schiff base on the right of Figure 1c). The third peak is also assigned to a C═N stretch, but in its nonconjugated form, which effectively causes the peak to shift to slightly higher wavenumbers (∼1658 cm^{-1}).[33] The last resolvable band in the double bond region is centered at ∼1715 cm^{-1} and assigned to the carbonyl stretch (C═O) from nonreacted aldehyde groups.

Although overall increasing, the relative intensities between these four bands change nonmonotonically with time, reflecting the intricacy of the cross-linking reaction. Moreover, and adding to this complexity, a decreasing fluorescent signal that overlapped with the Raman bands was observed during the early stages of the reaction. The fluorescence, which essentially vanished after approximately 40 min, indicates the presence of a highly conjugated intermediate in the interfacial region, capable of emitting fluorescent photons when excited with a 532 nm laser (the frequency of our source). The autofluorescense of glutaraldehyde solutions upon reaction with amine groups has been observed previously.[34] Note, however, that gluraldehyde in aqueous solutions is not fluorescent in the absence of compounds with amine functional groups (see, for instance, Figure S2 in Supporting Information).

Quantifying the amount of imine groups in the gel (i.e. cross-linking density) through analysis of the C═N stretching modes is thus not straightforward, as at least two different but, to some extent, also overlapping bands contribute to the overall intensity. In contrast, the isolated CH stretching band observed at 3102 cm^{-1} offers a much simpler solution (see Figure 2a). This peak, which we assign to the CH stretch of the hydrogen attached to the sp2 carbon in the imine group (H−C═N), is generally insensitive to whether the Schiff base is conjugated with the ethylenic double bond or not (note that the hydrogen attached to the C═C double bond gives rise to a significantly weaker band observed at ∼3050 cm^{-1}). The relative intensity of this band as a function of reaction time is shown in Figure 2b. The data was obtained using factor analysis[35] on a set of spectra collected during a 24 h period. Upon addition of glutaraldehyde, the cross-linking reaction proceeds rapidly, with half the total number of imine groups formed during the first 30 min. Ten additional hours are then required for the reaction to complete. It is worth noting the interlude in Schiff base formation observed between approximately 40 and 100 min (see Figure 2b). The commencement of this plateau coincides with the disappearance of the fluorescent intermediate, which thus appears to catalyze the cross-linking reaction. Moreover, it is also concurrent with the minimum in overall intensity observed for the saturated CH stretching modes between ∼2800 and 3000 cm^{-1} (see region in short segments in Figure 2a). All these elements confirm the complexity of the reaction mechanism, with formation of multiple intermediates following distinctive kinetics. A more in depth molecular insight into these intermediate reactions could, in principle, be obtained using TIRR by systematically varying the reaction conditions (i.e. glutaraldehyde concentration and solution pH). However, for the purpose of our chitosan-gel formation the end result is more relevant, that is the relative cross-linking density as a function of reaction time (see Figure 2b).

3.3. Formation of Surface Grafted Chitosan Gels upon Removal of PAA. As shown in Figure 2b, the number of imine bonds formed in the surface bound hydrogel film can be varied by the cross-linking reaction time. In this report we focus mainly on two different gels formed from 11/10 chitosan/PAA multilayers, referred to as LC-gels and HC-gels (where LC and HC stand for low and high cross-linked, respectively). The former is obtained after 20 min reaction time and corresponds to a film with a relative cross-linking density of ∼40%. The latter is obtained after 24 h and is equivalent to 100% relative cross-linking density. The reaction is interrupted by flushing the cell with a NaCl aqueous solution, followed by an overnight exposure to a buffer solution at pH 9. This facilitates the removal of trapped PAA from the cross-linked gel. The loss of PAA, as well as changes in the gel composition, was followed in situ with TIRR.

3.3.1. Molecular Information Obtained from TIRR. The TIRR spectra of a 11/10 chitosan/PAA multilayer, a LC-gel and a HC-gel, in contact with a 30 mM NaCl aqueous solution (pH = 5.7) are shown in Figure 3. Contributions from the silica substrate, as well as those from water molecules in the evanescent field, have been removed by subtraction using as reference the spectrum of the first adsorbed layer of chitosan.[13]

dx.doi.org/10.1021/la501319r | Langmuir 2014, 30, 8878−8888

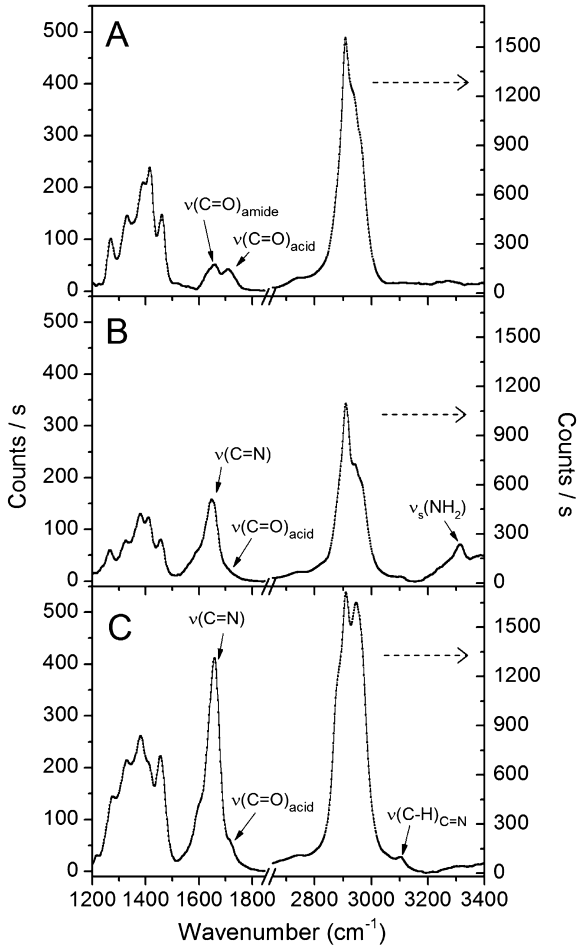

Figure 3. TIRR spectra of (a) the multilayer film consisting of 11 layers of chitosan and 10 of PAA prior to cross-linking, (b) LC-gel equivalent to a cross-linking density of 40%, and (c) HC-gel with a 100% relative cross-linking density measured in 30 mM NaCl at pH 5.7. Note the break in the spectra between 1825 cm^{-1} and 2650 cm^{-1}. For ease of comparison, the spectra at low and high frequency ranges are reported using two different absolute scales.

The spectral bands from the multilayer film (Figure 3a) have been described in detail in the first part of this series of papers[13] and only the most relevant peaks for the gel formation are discussed here. The multiple peaks observed between 1200−1500 cm^{-1} are mainly associated with wagging, twisting, and bending modes of methine and methylene groups found in both chitosan and PAA. The symmetric carboxylate stretch $\nu_s(COO^-)$ at 1420 cm^{-1} from the charged form of PAA is of particular interest, but it unfortunately closely overlaps with a bending mode of chitosan making it difficult to disentangle their individual contributions.[13] In the double bond stretching region (1580-1750 cm^{-1}), protonated PAA gives rise to a distinctive band at 1710 cm^{-1} assigned to the C═O stretch from the carboxylic functional group. As shown below, this peak will be relevant for determining the amount of PAA trapped inside the gel after the cross-linking reaction. In this spectral region an additional band centered at 1655 cm^{-1}, assigned to the C═O stretching of the amide in non-deacetylated segments of chitosan (15-25% of all sugar units), can also be clearly resolved (Figure 3a). The intensity of this band, however, remains unaltered in the subsequent stages, since the amide segments of chitosan neither participate in the cross-linking reaction with glutaraldehyde, nor are affected by the solution pH. Proceeding with the spectral assignments of the multilayer film, the multiple strong bands observed in the CH stretching region (2800−3000 cm^{-1}) are linked to contributions from both PAA and chitosan.

The spectrum of the LC-gel (Figure 3b) shows obvious differences when compared to the parent multilayer film. First, the imine and aldol-condensate peaks between 1590−1680 cm^{-1}, as well as the CH stretch from the imine group at 3100 cm^{-1} become apparent, indicating that the cross-linking reaction has indeed taken place (note that in Figure 3, spectral resolution was sacrificed in exchange of access to a wider spectral region. This is particularly evident when compared with Figure 2a). Second, in the OH stretching region a sharp peak, assigned to the symmetric NH_2 stretch from amine groups in chitosan, is clearly detected at 3315 cm^{-1}. The presence of this band is relevant for explaining the charging behavior of chitosan. In part I, no NH modes were observed at any stage of the multilayer build-up, implying that a large majority of, if not all, the amine groups in chitosan are found in their protonated form, most probably forming complexes with dissociated PAA segments.[13] Having as reference the strength of this band in the LC-gel spectrum, the detectability limit was estimated to be less than 5% at the end of the build-up process (i.e., at least 95% of the amine groups of chitosan are protonated before the multilayer is cross-linked). The appearance of NH modes in the LC-gel is mainly due to the significant removal of PAA from the gel, which facilitates deprotonation of NH_3^+ to NH_2. This is in spite of a 40% loss in the number of amine groups upon cross-linking. There is also a decrease in intensity in the CH stretching and fingerprint region bands relative to the multilayer film due to the removal of PAA from the surface grafted gel when exposed to a solution at pH 9. A close inspection of the spectrum in Figure 3b shows, however, that not all PAA is removed from the gel. This is evidenced by the shoulder observed at 1715 cm^{-1}, associated with the C═O stretch of the carboxylic group. As shown in the next section, the intensity of this band can actually be used to determine the relative amount of PAA trapped in the gel as a function of cross-linking density.

For the HC-gel (Figure 3c) the bands associated with the imine and aldol condensate groups formed during the cross-linking reaction are, as expected, significantly stronger. Moreover, the NH stretch at 3315 cm^{-1} is no longer visible in the spectrum, as all the amine groups from chitosan are consumed during the cross-linking reaction. Furthermore, and in contrast to the LC-gel, essentially no PAA is removed upon rinsing with the alkaline buffer solution. A close examination of the CH stretching region (2800−3000 cm^{-1}) in Figure 3c shows clear differences compared to that of the multilayer film prior to cross-linking (Figure 3a). The added intensity is due to CH contributions from the cross-linking agent as explicitly shown in Figure 2a.

3.3.2. Quantification of the Amount of PAA Trapped in the Surface Grafted Gels Using FTIR. The TIRR spectra for the LC- and HC-gels (Figure 3) show that PAA remains trapped in the gel, and that the amount remaining depends on the cross-linking density of the film. To gain further insight, we investigated a set of gel films with different cross-linking densities by means of transmission FTIR to quantify the amount of PAA removed after carbonate buffer rinsing (0.2 M, pH 9.2). FTIR is preferred over TIRR because the characteristic bands associated with PAA, specifically the asymmetric

dx.doi.org/10.1021/la501319r | *Langmuir* 2014, 30, 8878−8888

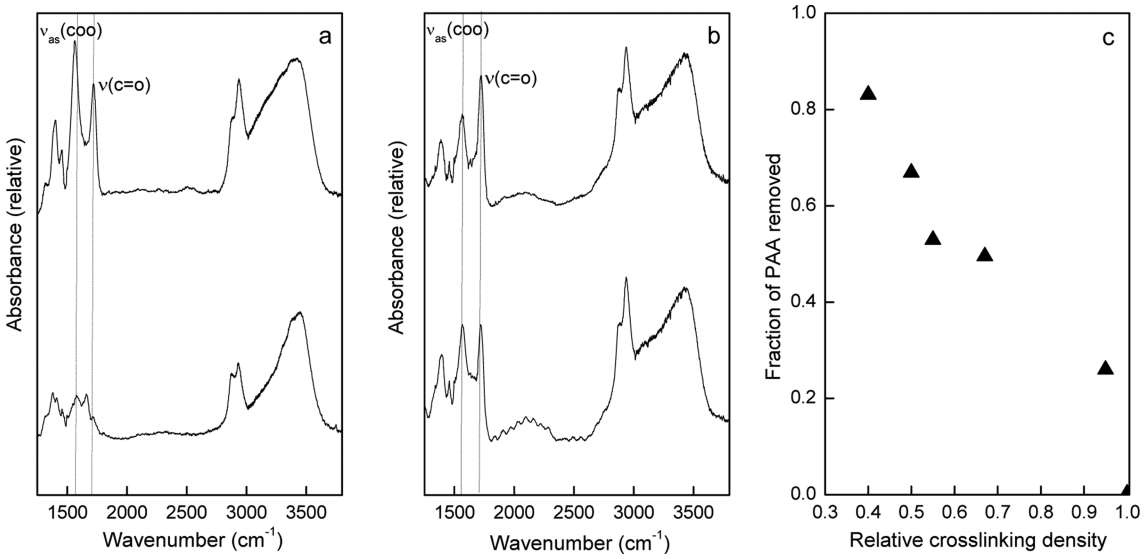

Figure 4. FTIR spectra of (a) a dried LC-gel and (b) a dried HC-gel. The upper spectra are measured before carbonate buffer rinsing, and the bottom spectra are measured after carbonate buffer rinsing. (c) Fraction of PAA removed by exposing the cross-linked multilayer structure to 0.2 M carbonate buffer at pH 9.2 as a function of cross-linking density.

carboxylate $\nu_{as}(COO^-)$ and carbonyl stretching $\nu(C{=}O)$ modes, have significantly higher cross sections in IR.[36] Concurrently, the IR cross sections from the partly overlapping C═N stretches in the imine groups are considerably lower,[37] making it easier to extract the individual PAA contributions from the spectra. Note, however, that in contrast to TIRR, the IR measurements were collected ex situ from dried films.

The FTIR spectra of dried LC- and HC-gels before (upper) and after (bottom) carbonate buffer rinsing are shown in Figure 4a and 4b. For the LC-gel, rinsing causes a significant signal drop in both the fingerprint and C−H stretching regions, consistent with the removal of PAA observed in the in situ TIRR measurements (Figure 3b). Accordingly, for the HC-gel rinsing does not have much effect on the integrated peak area.

The fraction of PAA removed by carbonate buffer rinsing can be determined by comparing the integrated areas of the carboxlate $\nu_{as}(COO^-)$ at 1580 cm^{-1} and the carboxylic acid $\nu(C{=}O)$ at 1710 cm^{-1} peaks before and after rinsing. These bands need to be considered together since PAA is found in both its protonated and deprotonated form in the gel. To this end, we utilize the Beer−Lambert law that can be written as

$$\Gamma = c \cdot l = A/\varepsilon \tag{3}$$

where Γ is the surface excess, c is the concentration, A is the absorbance, ε is the extinction coefficient, and l is the path length. Since the absorbance is proportional to the peak area, I_A, the relative amount of PAA in the gel can be estimated from eq 4, using the reported extinction coefficient ratio between the asymmetric carboxylate and carboxylic bands, $\varepsilon(\nu_{as(COO^-)})/\varepsilon(\nu_{(C=O)})$, of 2.4.[38]

$$\Gamma_{tot} = \Gamma_{coo-} + \Gamma_{c=o} \propto \frac{I_{A,coo-}}{\varepsilon_{coo-}} + \frac{I_{A,c=o}}{\varepsilon_{c=o}} \tag{4}$$

The fractions of PAA removed from different gels with varying cross-linking densities are shown in Figure 4c. The figure clearly shows that the fraction of PAA trapped inside the gel depends on the cross-linking density. For the LC-gel, equivalent to a cross-linking density of 40%, approximately 80% of the PAA can be removed by rinsing, while almost none can be removed from the HC-gel. Note that since contributions from unreacted aldehyde groups in the cross-linking agent (see, for example, Figures 1c and 2a) were neglected when calculating the intensity of the $\nu(C{=}O)$ band, the fractions reported in Figure 4c may be slightly underestimated.

3.3.3. Mass and Water Content of Gel Films. The water content in the LC and HC-gels was estimated using QCM-D as described in the experimental section. The dry masses of the two films were determined using the Johannsmann model (see Figure S3 in the Supporting Information for details). The large difference in mass between the two gels (Table 1) is in accordance with the results presented in Figure 4c that demonstrate that about 80% of the PAA is extracted for the LC-gel, whereas hardly any PAA leaves the HC-gel. For determining the wet mass, the Voigt model was proven to be more appropriate than the Johannsmann model as a clear nonlinearity makes the extrapolation to zero frequency difficult (see Supporting Information for details). The Voigt mass was estimated using the bulk viscosity (0.001 kg/ms) and density (1000 kg/m^3) of water as input parameters. Although affecting the calculated film thickness, the actual value chosen for the film density has no effect on the evaluated sensed mass. Table 1 summarizes the dry mass, sensed wet mass (evaluated using different models), as well as the water content of the ex situ prepared LC- and HC-gel films.

Table 1. Dry Mass (m_{dry}), Wet Mass (m_{wet}) Calculated Using the Sauerbrey (Third Overtone), Johannsmann, and Voigt Models (subscript "S", "J", and "V", respectively)

	m_{dry} (mg/m^2)	$m_{wet,S}$ (mg/m^2)	$m_{wet,J}$ (mg/m^2)	$m_{wet,V}$ (mg/m^2)	X_w[a]
LC-gel	57 ± 5	112 ± 5	117 ± 5	127 ± 5	0.55 ± 0.02
HC-gel	83 ± 5	134 ± 5	143 ± 5	155 ± 5	0.47 ± 0.02

[a]The water content, X_w was calculated based on the sensed mass obtained with the Voigt model.

dx.doi.org/10.1021/la501319r | *Langmuir* 2014, 30, 8878−8888

From the data in Table 1 we observe that the water content in the LC-gel is higher than in the HC-gel, which is a consequence of the higher cross-linking density in the latter. When a polymer gel particle is immersed in a good solvent, the osmotic pressure causes the solvent to diffuse into the gel, and this leads to swelling. The same is true for a gel layer, but here the swelling only occurs in one dimension, and it continuous until elastic forces in the cross-linked gel balance the osmotic pressure. The relatively small difference in water content between the two gels suggests that the swelling capability of the surface grafted gel is limited. This will be further discussed in section 3.4.

3.3.4. Topography of Surface Grafted Gels. AFM images illustrating the topography of the LC-and HC-gels in contact with air, are presented in Figure 5. The insets show zoomed-in sections of 2 × 2 μm^2, and height scan lines over the regions marked with straight lines are also included. Both gel surfaces are rough with peak-to-valley depths of about 30 nm. Island-like surface structures, with typical lateral dimension in the range 100−200 nm are observed, and such islands were also found for the multilayer film prior to cross-linking and extraction of PAA. As discussed in part I,[13] this is a consequence of the build-up mechanism. The root-mean-square roughness, R_q, is 22 nm over a 2 × 2 μm^2 area for both the LC- and HC-gels, indicating that the cross-linking time hardly affects the height variations. However, the scan lines show that the height changes occur in a more smooth fashion for the HC-gel on the 10−100 nm length scale.

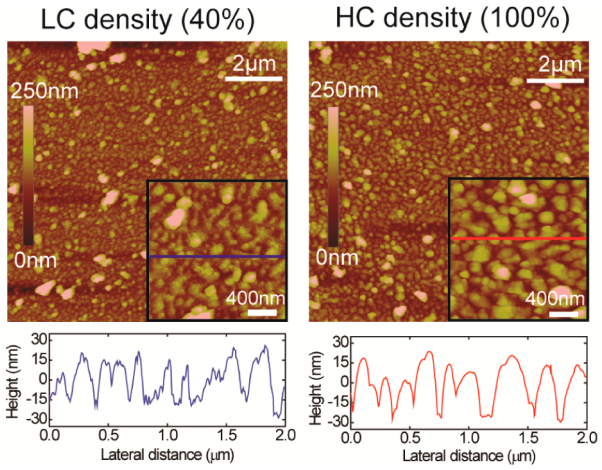

Figure 5. AFM topography images (10 × 10 μm^2) of the LC-gel (left) and HC-gel (right) determined in air. The insets show zoomed in sections of 2 × 2 μm^2, and height scan lines over the regions marked with a straight line are also provided. Samples were studied ex situ.

3.4. Stimuli Responses. *3.4.1. Responses to pH Changes.* Polyelectrolyte gels bearing weak acidic or basic groups display pH-induced volume transitions. For instance, the protonation of amine groups of a chitosan gel upon lowering the pH causes an increase in counterion concentration in the gel as well as in the electrostatic repulsion between the cationic segments, which leads to swelling. In this work we use QCM-D and TIRR to monitor the response of LC- and HC-gel layers, as well as the reversibility of the response. In these experiments the ionic strength of the solution was kept constant at 30 mM.

The frequency and dissipation changes observed for the LC- and HC-gels when the solution pH was changed repeatedly between 5.7 and 2.7 are reported in Figure 6. The layer swells at pH 2.7, which results in a decrease in frequency due to uptake of water and ions, as well as an increase in dissipation due to reduced rigidity and larger thickness. As proven by TIRR in the following section, the swelling results from an increased ionization of the amine groups in chitosan, and as well an increased protonation of carboxylic acid groups in the remaining PAA, causing a charge imbalance in the film. A significantly larger response is observed for the LC-gel, demonstrating more extensive swelling for the less cross-linked gel film. This is as expected since the swelling process stops when the osmotic pressure difference between bulk solution and gel layer is balanced by the retractive force that originates from the entropic penalty of elastically stretching the polymer chains between the cross-linking points.

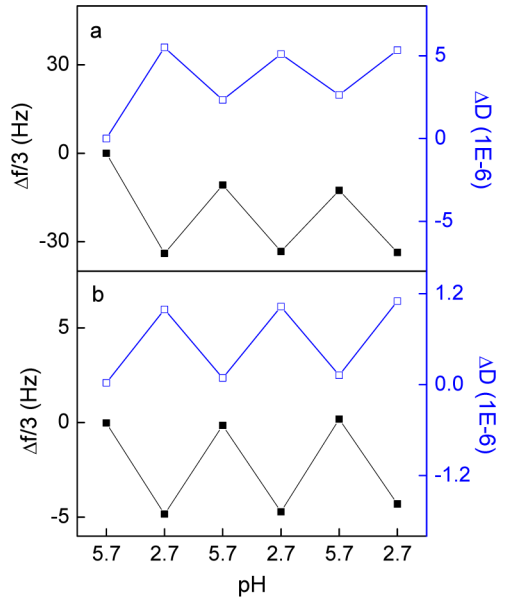

Figure 6. Frequency and dissipation change as a function of pH during repeated changes between pH 5.7 and 2.7 measured in 30 mM NaCl. Data for the LC-gel (a) and for the HC-gel (b). Black points represent frequency, and blue open squares represent dissipation.

The response of the HC-gel film is always reversible. However, for the LC-gel film the response during the first cycle of pH change is different (see Figure 6a). When pH is changed back to 5.7 from 2.7, neither the frequency nor the dissipation comes back to the starting value. This suggests that after exposure to the acidic solution, either a new conformation of the LC-gel with more water is achieved, or a portion of the PAA molecules originally trapped in the layer diffuse out during exposure to the acidic solution. The reversible mass change experienced during pH-cycles, calculated with the Voigt model, is 5 mg/m^2 and 1 mg/m^2 for the LC- and HC-gels, respectively. It is worth noting that these changes correspond to variations in the film thickness of barely 3.5% for the LC-gel, and less than 1% for the HC-gel.

TIRR was used to further understand the cause of the irreversible response of the LC-gel during the first pH cycle. The corresponding spectra are shown in Figure 7. A number of interesting conclusions can be extracted from the data: first, the intensity of the C−H stretching peaks between 2800 to 3000 cm^{-1} remains constant indicating that no polyelectrolyte is lost during the process. Thus, we can disregard the hypothesis that

dx.doi.org/10.1021/la501319r | Langmuir 2014, 30, 8878−8888

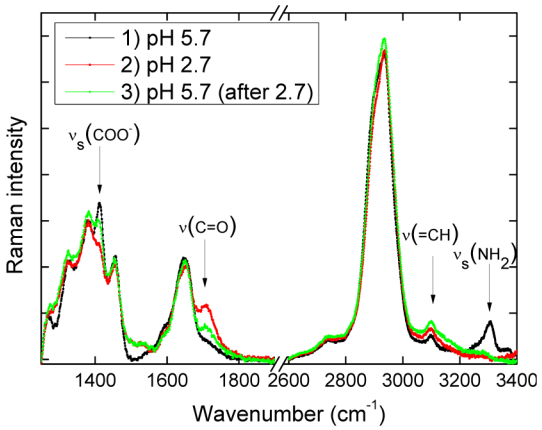

Figure 7. TIRR spectra of the LC-gel during the first pH cycle: 5.7 in black →2.7 in red →5.7 in green. Background electrolyte: 30 mM NaCl solution. Note the break in the spectra between 1850 cm^{-1} and 2600 cm^{-1}. Contributions from the silica substrate and water molecules in the evanescent field have been subtracted using as reference the spectrum of the first adsorbed layer of chitosan.

some PAA diffuses out of the film when exposed to a solution of pH 2.7. Second, the exposure to acidic solution does not change the degree of cross-linking as the intensity of the peak at 3102 cm^{-1} ($\nu_{=CH}$), associated with the cross-linking agent, also remains approximately constant. Third, the proportion of protonated amine groups in chitosan, as well as deprotonated carboxylate groups in PAA varies irreversibly during the first cycle. Before exposure to the acidic solution, the amine band from chitosan at 3315 cm^{-1} is clearly detected, while only a small shoulder at 1710 cm^{-1} from the carbonyl band of protonated PAA is observed, indicating that a large fraction of the remaining PAA in the gel is charged (black spectrum in Figure 7). When the solution pH is reduced to 2.7, the amine peak disappears, while the carbonyl band increases. At the same time the intensity of the symmetric carboxylate peak at 1420 cm^{-1}, associated with the charged form of PAA, decreases. These changes are expected since it is anticipated that at low pHs both the amine groups from chitosan and carbonyl groups in PAA will be found in their protonated forms (i.e., NH_2 → NH_3^+ and COO^- → COOH). When the pH is returned to 5.7, however, the amine band remains largely absent, and neither the carboxylate nor the carbonyl peak intensities return to their original values (green spectrum in Figure 7). The system behaves as if the pH inside the gel was lower than at the starting conditions, this in spite of having identical bulk pHs. With a larger fraction of $-NH_3^+$ groups, more counterions and water molecules are expected inside the gel, explaining the higher sensed mass detected by QCM-D after the first pH cycle (Figure 6a). It is worth noting that the TIRR spectra becomes reversible after the first pH cycle, indicating that a structural change indeed takes place inside the film, when exposed for the first time to acidic conditions.

3.4.2. Determining the pK_a Values of the LC-Gel Using TIRR. The apparent pK_a for chitosan, as well as that from the remaining PAA in the LC-gel can be determined using TIRR. This is accomplished by measuring the relative intensity of specific peaks as a function of pH. For chitosan, the targeted band is the NH_2 symmetric stretch at 3315 cm^{-1}, which vanishes under acidic conditions once all amine groups become protonated (NH_2 → NH_3^+). For PAA, both the carboxylate (COO^-) symmetric stretching band at 1420 cm^{-1}, as well as the carbonyl (C═O) stretching band at 1710 cm^{-1} can be used, giving additional confidence in the determined pK_a values for PAA. The relative intensities of these three bands as a function of pH are shown in Figure 8. The values are obtained from Lorenztian fits of the concerned peaks, as discussed in more detail in the Supporting Information. From Figure 8a,b it is evident that chitosan and PAA have each two distinctive pK_a values, which can be estimated by fitting the data to eq 5 (solid curves in Figure 8):

$$\text{Relative Intensity} = \beta_1 \frac{(10^{\text{pH}-\text{p}K_{a1}})}{1 + (10^{\text{pH}-\text{p}K_{a1}})} + \beta_2 \frac{(10^{\text{pH}-\text{p}K_{a2}})}{1 + (10^{\text{pH}-\text{p}K_{a2}})} \quad (5)$$

where, β_1 and β_2 are the fraction of chargeable groups having a pK_{a1} and a pK_{a2} value, respectively. The determined parameters are summarized in Table 2.

The fact that both chitosan and PAA have two populations with chargeable groups (i.e., amine and carboxylic acid) with distinct pK_a values is somewhat intriguing (Table 2). Two of the determined pK_a's, p$K_{a1}^{(chitosan)}$ and p$K_{a2}^{(PAA)}$, lie in the range of those expected from bulk aqueous solutions of the corresponding polyelectrolytes (6.0−6.5 for chitosan,[39,40] and 4.3−6.5 for PAA.[39,41,42]), which make their interpretation rather straightforward. Nonetheless, a suitable explanation for the two remaining pK_a's, which differ significantly from those in the bulk, requires additional considerations. The fact that p$K_{a2}^{(chitosan)}$ and p$K_{a1}^{(PAA)}$ shift in opposite directions from those in the bulk, discards the possibility of justifying the

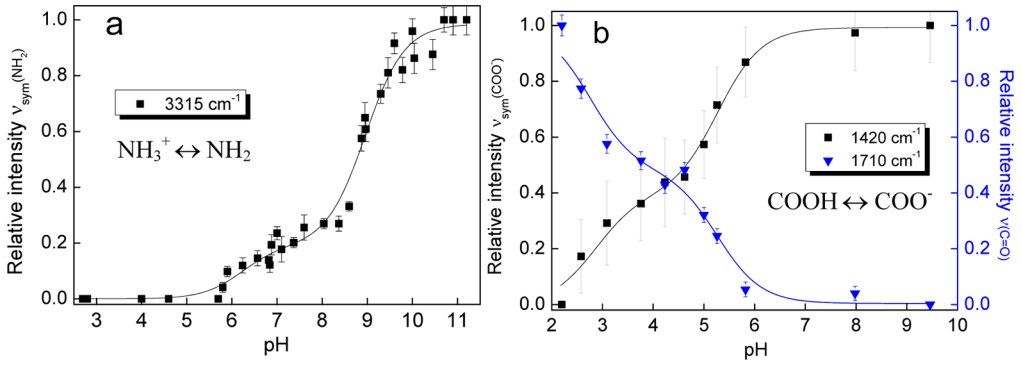

Figure 8. Relative proportion of (a) amine (NH_2) groups in chitosan and (b) carbonyl (blue triangles) and carboxylate (black squares) groups in PAA as a function of pH (see text for details). Solid curves are fits to the data calculated using eq 5.

dx.doi.org/10.1021/la501319r | Langmuir 2014, 30, 8878−8888

Table 2. pK_a Values for Chitosan and PAA in the LC-Gel, Determined from Fitting the Data Shown in Figure 8[a]

chitosan		PAA	
pK_{a1}	6.2 ± 0.3	pK_{a1}	2.8 ± 0.3
$\beta_1(pK_{a1})$	0.20 ± 0.03	$\beta_2(pK_{a1})$	0.5 ± 0.1
pK_{a2}	9.0 ± 0.1	pK_{a2}	5.3 ± 0.3
$\beta_2(pK_{a2})$	0.80 ± 0.03	$\beta_2(pK_{a2})$	0.5 ± 0.1

[a]The fraction of chargeable groups, β_x (pK_{ax}), having a specific pK_{ax} are also shown in the table. The values for PAA are obtained by averaging the individual results from the carbonyl and carboxylate bands.

phenomenon by a variation in the surface concentration of hydronium ions.[43] The early deprotonation of a fraction of carboxylic groups from PAA ($pK_{a1}^{(PAA)}$ = 2.8) can instead be explained by the formation of an ionic complex with neighboring protonated amino group in chitosan ($NH_3^+ \leftrightarrow COO^-$). Equivalently, the second pK_a in chitosan ($pK_{a2}^{(chitosan)}$ = 9.0) would originate from the deprotonation of the NH_3^+ groups in the same complexes, resulting in their rupture at higher pHs. Support for this mechanism can be found in the swelling behavior as a function of pH of chitosan/PAA complexes formed in the bulk, where two distinct swelling transitions have been reported between pH 2−3 (deswelling) and pH 8−10 (swelling).[39,40] In this line of thought, the LC-gel will be expected to swell not only at low pHs, when the amine groups in chitosan are protonated as shown in Figure 7, but also for pHs higher than 9, when both the PAA and chitosan are deprotonated (COO^- and NH_2). This is indeed observed by QCD-D as shown in the Supporting Information.

It is worth noting that the fraction of amine groups in chitosan displaying a pK_a of 9.0 cannot all be forming complexes with PAA in the LC-gel. From the fitted fractions of the two populations of amine groups in chitosan, β_1 (pK_{a1}) and β_2 (pK_{a2}) in Table 2, together with the fact that 40% of the original number of amine groups in the multilayer are consumed during the cross-linking reaction (Figure 2b), the relative amount of chargeable monomeric units in chitosan available for complexating with PAA in the LC-gel can be estimated. On the other hand, when considering that ∼80% of PAA originally present[13] in the multilayer is removed after rinsing the cross-liked gel (see Figure 4c), the total number of amine groups in chitosan with an apparent $pK_a^{(chitosan)}$ of 9.0, relative to all available carboxylate groups in PAA is ∼2:1. One possibility is that the remaining amine groups from chitosan having a pK_a of 9.0 form complexes with the dissociated silanol groups (SiO^-) from the underlying silica substrate.

3.4.3. Response to Ionic Strength Changes. As deduced from Figure 8a, the amine groups in chitosan are fully charged at pH 2.7. Thus, the degree of ionization is not expected to be significantly affected by an increase in the bulk ionic strength. On the other hand, an increase in ionic strength screens electrostatic interactions, and this could lead to shrinkage of the gel film. The data provided in Figure 9 illustrate that neither the LC- nor the HC-gel layer show any significant response when the NaCl concentration is varied between 10 and 100 mM at pH 2.7. This lack of response to ionic strength changes suggests that the cationic chitosan charges present in the hydrogel are largely compensated by negatively charged species, mainly chloride ions in our case, present within the gel throughout the investigated ionic strength interval.

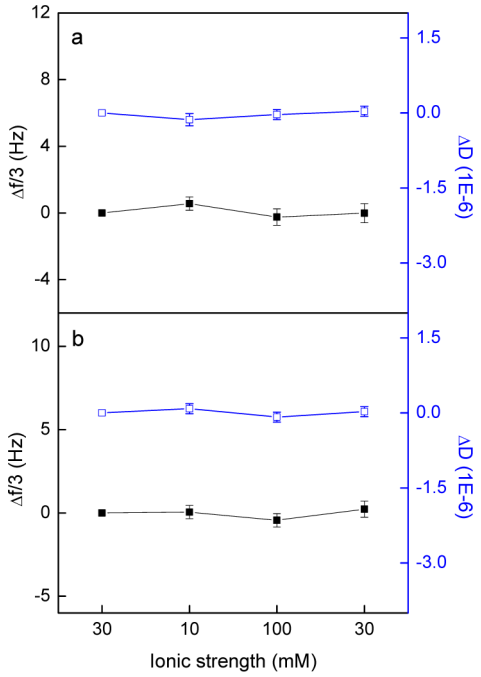

Figure 9. Changes in frequency and dissipation as a result of changes in ionic strength for a LC-gel layer (a) and a HC-gel layer (b) at pH 2.7. The ionic strength was regulated by addition of NaCl. Black points represent frequency, and blue points represent dissipation.

This further suggests that the excess charge in the gel layer is small and that the effective surface charge density of the gel layer that determines the strength of double-layer forces between the gel and another charged surface or particle may be relatively small and not affected by pH and ionic strength changes. We will discuss this further in the subsequent paper of this series where pH and ionic strength effects on surface forces and friction forces between a gel layer and a silica surface will be reported.

4. SUMMARY AND CONCLUDING REMARKS

We have successfully made surface-grafted gels with different cross-linking densities on silica surfaces. Chemical cross-linking the amine groups in chitosan, using gluteraldehyde as the cross-linking agent, improves the stability of the film toward changes in solution pH and ionic strength. TIRR allowed tracking in situ the cross-linking reaction and quantitatively determine the relative cross-linking density as a function of reaction time. The data showed that the reaction mechanism is complex, with formation of multiple intermediates following distinctive kinetics. Although not involved in the cross-linking reaction, poly(acrylic) acid was found to remain trapped in the gel layer even after exposure to a high pH solution. The amount of PAA remaining was found to increase with increasing cross-linking density as determined in situ by TIRR and ex situ by FTIR.

The surface grafted gels are responsive to pH changes, but not to changes in ionic strength (between 10 and 100 mM at pH 2.7). The absence of response to ionic strength changes is suggested to be due to the large concentration of counterions within the gel. When the solution pH is alternated between 2.7 and 5.7 (in 30 mM NaCl), highly cross-linked gels show a fully reversible swelling/deswelling behavior. In contrast, gels that are less cross-linked (40%) display a larger pH-response, but reversible behavior is only observed after the first exposure to

dx.doi.org/10.1021/la501319r | Langmuir 2014, 30, 8878−8888

the acidic solution. TIRR measurements show that this is due to changes in the gel structure that results in more protonated amines and carboxylate groups when the pH is returned to 5.7 compared to at this pH-value prior to exposure to the pH 2.7 solution.

Interestingly, we find by TIRR analysis that amine groups from chitosan and the carboxylic groups from the remaining PAA in the low cross-linked gel have each two distinctive pK_a values. For chitosan they are 6.2 (similar to in bulk solution) and 9.0. For PAA in the same gel the determined pK_a's are 2.8 and 5.3, with the latter in the expected range for PAA in bulk solution. The first p*K*a of 2.8 for PAA is attributed to the deprotonation of carboxylate groups upon formation of an ionic complex with neighboring protonated amino group in chitosan. The second pK_a (9.0) for chitosan is in turn largely explained by the rupture of the same polyelectrolyte complex with PAA or with the undelying silica surface.

■ ASSOCIATED CONTENT

Ⓢ Supporting Information

Bulk Raman spectra of glutaraldehyde, determination of the dry and wet mass of the surface grafted gels using QCM, estimating the gel pK_a's using TIRR, and swelling behavior of the LC-gel at basic pHs. This material is available free of charge via the Internet at http://pubs.acs.org/.

■ AUTHOR INFORMATION

Corresponding Author

*E-mail: tyrode@kth.se.

Notes

The authors declare no competing financial interest.

■ ACKNOWLEDGMENTS

All authors acknowledge individual financial support from the Swedish Research Council, VR. E.Th. and E.Ty. also acknowledge support from the Swedish Foundation for Strategic Research (SSF) through the programs "Microstructure, Corrosion and Friction Control" and "Future Research Leaders-5", respectively.

■ REFERENCES

(1) Tokarev, I.; Minko, S. Stimuli-Responsive Hydrogel Thin Films. *Soft Matter* **2009**, *5* (3), 511−524.

(2) Stuart, M. A. C.; Huck, W. T. S.; Genzer, J.; Muller, M.; Ober, C.; Stamm, M.; Sukhorukov, G. B.; Szleifer, I.; Tsukruk, V. V.; Urban, M.; Winnik, F.; Zauscher, S.; Luzinov, I.; Minko, S. Emerging Applications of Stimuli-Responsive Polymer Materials. *Nat. Mater.* **2010**, *9* (2), 101−113.

(3) Dédinaité, A. Interfacial Properties of Mucins. In *Encyclopedia of Surface and Colloid Science*, 2nd ed.; Taylor & Francis: Boca Raton, FL, 2007; pp 1−17.

(4) Mow, V. C.; Holmes, M. H.; Michael Lai, W. Fluid Transport and Mechanical Properties of Articular Cartilage: A Review. *J. Biomech.* **1984**, *17* (5), 377−394.

(5) Mansour, J. M. In *Kinesiology: The Mechanics and Pathomechanics of Human Movement*; Lippincott Williams and Wilkins: Philadelphia, PA, 2003.

(6) Liu, C.; Wang, M.; An, J.; Thormann, E.; Dedinaite, A. Hyaluronan and Phospholipids in Boundary Lubrication. *Soft Matter* **2012**, *8* (40), 10241−10244.

(7) Badawy, M. E. I.; Rabea, E. I.; Rogge, T. M.; Stevens, C. V.; Smagghe, G.; Steurbaut, W.; Hofte, M. Synthesis and Fungicidal Activity of New N,O-Acyl Chitosan Derivatives. *Biomacromolecules* **2004**, *5* (2), 589−595.

(8) Rabea, E. I.; Badawy, M. E. T.; Stevens, C. V.; Smagghe, G.; Steurbaut, W. Chitosan as Antimicrobial Agent: Applications and Mode of Action. *Biomacromolecules* **2003**, *4* (6), 1457−1465.

(9) Yamamoto, H.; Amaike, M. Biodegradation of Cross-Linked Chitosan Gels by a Microorganism. *Macromolecules* **1997**, *30* (13), 3936−3937.

(10) Zhao, Z. M.; He, M.; Yin, L. C.; Bao, J. M.; Shi, L. L.; Wang, B. Q.; Tang, C.; Yin, C. H. Biodegradable Nanoparticles Based on Linoleic Acid and Poly(*β*-malic acid) Double Grafted Chitosan Derivatives as Carriers of Anticancer Drugs. *Biomacromolecules* **2009**, *10* (3), 565−572.

(11) Hu, Q. L.; Li, B. Q.; Wang, M.; Shen, J. C. Preparation and Characterization of Biodegradable Chitosan/Hydroxyapatite Nanocomposite Rods via in Situ Hybridization: A Potential Material as Internal Fixation of Bone Fracture. *Biomaterials* **2004**, *25* (5), 779−785.

(12) Sashiwa, H.; Yajima, H.; Aiba, S. Synthesis of a Chitosan−Dendrimer Hybrid and Its Biodegradation. *Biomacromolecules* **2003**, *4* (5), 1244−1249.

(13) Liu, C.; Thormann, E.; Claesson, P. M.; Tyrode, E. Surface Grafted Chitosan Gels. Part I: Molecular Insight into the Formation of Chitosan and Poly(acrylic acid) Multilayers. *Langmuir* **2014**, DOI: 10.1021/la5013186.

(14) Goissis, G.; Junior, E. M.; Marcantonio, J. A. C.; Lia, R. C. C.; Cancian, D. C. J.; de Carvalho, M. Biocompatibility Studies of Anionic Collagen Membranes with Different Degree of Glutaraldehyde Cross-Linking. *Biomaterials* **1999**, *20* (1), 27−34.

(15) Boudou, T.; Crouzier, T.; Auzély-Velty, R.; Glinel, K.; Picart, C. Internal Composition versus the Mechanical Properties of Polyelectrolyte Multilayer Films: The Influence of Chemical Cross-Linking. *Langmuir* **2009**, *25* (24), 13809−13819.

(16) Bechler, S. L.; Lynn, D. M. Reactive Polymer Multilayers Fabricated by Covalent Layer-by-Layer Assembly: 1,4-Conjugate Addition-Based Approaches to the Design of Functional Biointerfaces. *Biomacromolecules* **2012**, *13* (5), 1523−1532.

(17) Bongaerts, J. H. H.; Cooper-White, J. J.; Stokes, J. R. Low Biofouling Chitosan-Hyaluronic Acid Multilayers with Ultra-Low Friction Coefficients. *Biomacromolecules* **2009**, *10* (5), 1287−1294.

(18) Wang, B.-l.; Ren, K.-f.; Chang, H.; Wang, J.-l.; Ji, J. Construction of Degradable Multilayer Films for Enhanced Antibacterial Properties. *ACS Appl. Mater. Interfaces* **2013**, *5* (10), 4136−4143.

(19) Zhang, Y. J.; Guan, Y.; Zhou, S. Q. Single Component Chitosan Hydrogel Microcapsule from a Layer-by-Layer Approach. *Biomacromolecules* **2005**, *6* (4), 2365−2369.

(20) Suto, S.; Ui, N. Chemical Crosslinking of Hydroxypropyl Cellulose and Chitosan Blends. *J. Appl. Polym. Sci.* **1996**, *61* (13), 2273−2278.

(21) Tyrode, E.; Liljeblad, J. F. D. Water Structure Next to Ordered and Disordered Hydrophobic Silane Monolayers: A Vibrational Sum Frequency Spectroscopy Study. *J. Phys. Chem. C* **2013**, *117* (4), 1780−1790.

(22) Woods, D. A.; Bain, C. D. Total Internal Reflection Raman Spectroscopy. *Analyst* **2012**, *137* (1), 35−48.

(23) Tyrode, E.; Rutland, M. W.; Bain, C. D. Adsorption of CTAB on Hydrophilic Silica Studied by Linear and Nonlinear Optical Spectroscopy. *J. Am. Chem. Soc.* **2008**, *130* (51), 17434−17445.

(24) Saurbrey, G. Verwendung von Schwingquarzen zur Wagung Dunner Schichten und zur Mikrowagung. *Z. Phys.* **1959**, *155*, 206.

(25) Voinova, M. V.; Rodahl, M.; Jonson, M.; Kasemo, B. Viscoelastic Acoustic Response of Layered Polymer Films at Fluid-Solid Interfaces: Continuum Mechanics Approach. *Phys. Scr.* **1999**, *59* (5), 391.

(26) Johannsmann, D.; Mathauer, K.; Wegner, G.; Knoll, W. Viscoelastic Properties of Thin-Films Probed with a Quartz-Crystal Resonator. *Phys. Rev. B* **1992**, *46* (12), 7808−7815.

(27) Kovacevic, D.; van der Burgh, S.; de Keizer, A.; Cohen Stuart, M. A. Kinetics of Formation and Dissolution of Weak Polyelectrolyte Multilayers: Role of Salt and Free Polyions. *Langmuir* **2002**, *18* (14), 5607−5612.

(28) Dubas, S. T.; Farhat, T. R.; Schlenoff, J. B. Multiple Membranes from "True" Polyelectrolyte Multilayers. *J. Am. Chem. Soc.* **2001**, *123* (22), 5368−5369.
(29) Migneault, I.; Dartiguenave, C.; Bertrand, M. J.; Waldron, K. C. Glutaraldehyde: Behavior in Aqueous Solution, Reaction with Proteins, and Application to Enzyme Crosslinking. *BioTechniques* **2004**, *37* (5), 790−802.
(30) Kildeeva, N. R.; Perminov, P. A.; Vladimirov, L. V.; Novikov, V. V.; Mikhailov, S. N. About Mechanism of Chitosan Cross-Linking with Glutaraldehyde. *Russ. J. Bioorg. Chem.* **2009**, *35*, 360−369.
(31) Monsan, P.; Puzo, G.; Mazarguil, H. Étude du Mécanisme d'Établissement des Liaisons Glutaraldéhyde-Protéines. *Biochimie* **1976**, *57* (11−12), 1281−1292.
(32) Margel, S.; Rembaum, A. Synthesis and Characterization of Poly(glutaraldehyde). A Potential Reagent for Protein Immobilization and Cell Separation. *Macromolecules* **1980**, *13* (1), 19−24.
(33) Colthup, N.; Daly, L. H.; Wiberley, S. E. *Introduction to Infrared and Raman Spectroscopy*, 3rd ed.; Academic Press: San Diego, CA, 1990; p 547.
(34) Lee, K.; Choi, S.; Yang, C.; Wu, H.-C.; Yu, J. Autofluorescence Generation and Elimination: A Lesson from Glutaraldehyde. *Chem. Commun.* **2013**, *49* (29), 3028−3030.
(35) Malinowski, E. R. *Factor Analysis in Chemistry*, 3rd ed.; Wiley: New York, 2002.
(36) Bardet, L.; Cassanas-Fabre, G.; Alain, M. Étude de la Transition Conformationnelle de l'Acide Polyacrylique Syndiotactique en Solution Aqueuse par Spectroscopie de Vibration. *J. Mol. Struct.* **1975**, *24* (1), 153−164.
(37) Bellamy, L. J. In *The Infrared Spectra of Complex Molecules*; Chapman & Hall: London/New York, 1980.
(38) Leyte, J. C.; Zuiderweg, L. H.; Vledder, H. J. An I.R. Investigation of Polyion−Counterion Interactions. *Spectrochim. Acta, Part A: Mol. Spectrosc.* **1967**, *23* (5), 1397−1407.
(39) Argüelles-Monal, W.; Peniche-Covas, C. Study of the Interpolyelectrolyte Reaction between Chitosan and Carboxymethyl Cellulose. *Makromol. Chem., Rapid Commun.* **1988**, *9* (10), 693−697.
(40) Rinaudo, M.; Pavlov, G.; Desbrières, J. Influence of Acetic Acid Concentration on the Solubilization of Chitosan. *Polymer* **1999**, *40* (25), 7029−7032.
(41) Choi, J.; Rubner, M. F. Influence of the Degree of Ionization on Weak Polyelectrolyte Multilayer Assembly. *Macromolecules* **2004**, *38* (1), 116−124.
(42) Kajiwara, K.; Ross-Murphy, S. B. Synthetic Gels on the Move. *Nature* **1992**, *355* (6357), 208−209.
(43) Israelachvili, J. N. *Intermolecular and Surface Forces*, 3rd ed.; Elsevier: Oxford, U.K., 2011; p 674.